Light Diffraction of *in vitro* Crystals of Six Tobacco Mosaic Viruses

U. Kreibig and C. Wetter

Department of Experimental Physics and Department of Botany, Universität des Saarlandes, D-6600 Saarbrücken

Z. Naturforsch. **35 c,** 750–762 (1980); received March 7, 1980

Tobacco Mosaic Viruses, Crystallization, Phase Transitions, Light Diffraction, Crystal Structure, Model Calculations

Iridescent gels of the common, tomato mosaic, para-tobacco mosaic, ribgrass mosaic, sunnhemp mosaic, and cucumber 4 tobacco mosaic virus strains were prepared using the purification method of Boedtker and Simmons (J. Amer. Chem. Soc. 1958). Macrocrystals which were stable for many months could be grown from iridescent gels of all viruses when stored at 0–10 °C. The gels exhibited various structural phases (nematic and smectic) differing in density. The structure of the microcrystalline gels and of macrocrystals was investigated by means of optical diffraction. Distinct Bragg reflections were observed from which a *mean* periodicity of 340 nm was derived for all virus strains. The results indicate a crystalline multilayer structure as first proposed by Oster (J. Gen. Physiol. **33,** 445, [1950]). The angular positions and widths of the Bragg reflections depended on the concentration of virus and the ionic strength. The periodicity decreased from 365 nm at 30 mg/ml virus to about 315 nm at 109 mg/ml virus, *i. e.* the periodicity approached the 300 nm length of the virion. Model calculations taking into account Debye-Hückel repulsive and van der Waals attractive forces gave a qualitative explanation for the crystalline structure and its observed concentration dependence. The *in vitro* crystals resemble immature crystal forms observed in the living cell.

Introduction

The discovery of the liquid crystalline properties of concentrated (> 2%) tobacco mosaic virus (TMV) preparations [1] has stimulated detailed studies including the use of X-ray diffraction methods [2] as well as theoretical investigations [3]. Early microscopical work [4, 5] was done in order to compare crystal forms obtained from purified preparations with those produced by the living cell. The crystalline phases obtained *in vitro*, however, were paracrystalline (nematic) and not of two-dimensional (smectic) order like the abundant hexagonal crystals occurring *in vivo* [6–8].

On the other hand, smectic arrays were observed when virus was dried from solution [9] or after precipitation with basic proteins [10]. Oster [11] first reported the formation of three-dimensional crystallites separating from the anisotropic bottom layer of purified TMV, both of the common and the Holmes ribgrass strains. Because of the diffraction of visible light this smectic phase was called "iridescent gel". By measuring the reflection angle at a given wavelength, the distance of the reflecting planes in the crystallites was determined according to Bragg's law. In a model to explain this periodicity it was suggested that layers of virions, orientated parallel and with the ends aligned, are separated by layers of water.

We report here on an easy way to prepare iridescent gels and on the formation of large single liquid crystals of 6 tobamoviruses [12]. The periodic layer structure was determined by measuring the diffraction of laser light of different wavelengths. The results will be discussed with respect to the theory of repulsive-attractive long-range forces acting between the TMV particles within the crystal. Similar studies have been made on the crystal structure of tipula iridescent virus [13].

Reprint requests to Prof. Dr. C. Wetter.
0341-0382/80/0900-0750 $ 01.00/0

Materials and Methods

Purification of viruses

The 6 tobamoviruses used in the experiments and the hosts in which they were propagated are listed in Table I. In order to obtain virus preparations of essentially uniform particle length [14] the purification procedure of Boedtker and Simmons [15] (B & S method) was used. If necessary, green host material could be removed by a second treatment with Celite after the second high speed run. As CV 4 became increasingly insoluble in distilled water after several centrifugations, it was dissolved in 0.01 M phosphate

Table I. Tobamoviruses and host plants used for crystallization experiments.

Virus	Host plant	Original sources
Tobacco mosaic virus (TMV), common strain=U1	*Nicotiana tabacum* cv. Samsun, White Burley *N. sylvestris*	H. G. Wittmann
Tomato mosaic virus (ToMV) dahlemense strain	*N. tabacum* var. Samsun	G. Melchers
Para-tobacco mosaic virus (PTMV), = U2 strain	*N. tabacum* var. Samsun	own isolate
Ribgrass mosaic virus (HRV), Holmes' strain	*N. tabacum* var. Samsun	F. O. Holmes
Sunn-hemp mosaic virus (CPV), cowpea strain	*Phaseolus vulgaris* different cultivars	F. C. Bawden
Cucumber virus 4 (CV4)	*Cucumis vulgaris* different cultivars	A. C. Knight

buffer pH 7.2, except after the last cycle, when distilled water was used.

For comparison, virus was purified by clarifying the expressed sap with 1:5 (v/v) chloroform-butanol (1:3 v/v) and by precipitation with polyethylene glycol and NaCl (both 4% w/v) or ammonium sulfate (30% saturation) before centrifugation. Virus concentrations were determined spectrophotometrically using an extinction coefficient of 3.06 ($E^{0.1\%}_{1\,\mathrm{cm},\ 260\,\mathrm{nm}}$ uncorrected for light scattering) or by measuring the refractive index and using a value for the specific refractive index increment dn/dc of 0.194 ml g^{-1} [15]. The conductivity of virus preparations was measured in a cell with a cell constant of 0.43 cm^{-1}, using the Philips PW 9501 conductivity bridge. Our samples of distilled water had conductivities of 3.1–5.4 μS cm^{-1}.

Light diffraction apparatus

The apparatus used to measure the angle and the angular width of the light diffracted by TMV crystals, is shown in Fig. 1.

Radiation sources were an Ar-Laser (Coherent Radiation Mod. 52) and a He-Ne-Laser, and so the following wavelengths (nm) were available: 632.8, 514.5, 501.7, 496.5, 488.0, 476.5 and 472.5. The beam diameter was ~ 1.5 mm at the $1/e^2$ points; its divergence was about 0.8 m rad.

Iridescent gels were studied in two kinds of cells. The first kind (type A) were glass tubes ($Ø_i \simeq 2$ mm, $Ø_a \simeq 3.5$ mm), filled with the gel which were put into a cuvette filled with water, as shown in Fig. 1. This cuvette, consisting of one plane and one semicylindric window, was used to reduce astigmatic focusing of the beam by the glass tube. Nevertheless, the difference between the refractive indices of water and of glass, caused the scattered beam to become slightly divergent. Additional divergence was brought about by the spatial extension of the scattering volume. Numerical geometric-optic computations for several selected rays through the cuvette system gave an effective angle of divergence of about 8 m rad. A slight net refraction of the scat-

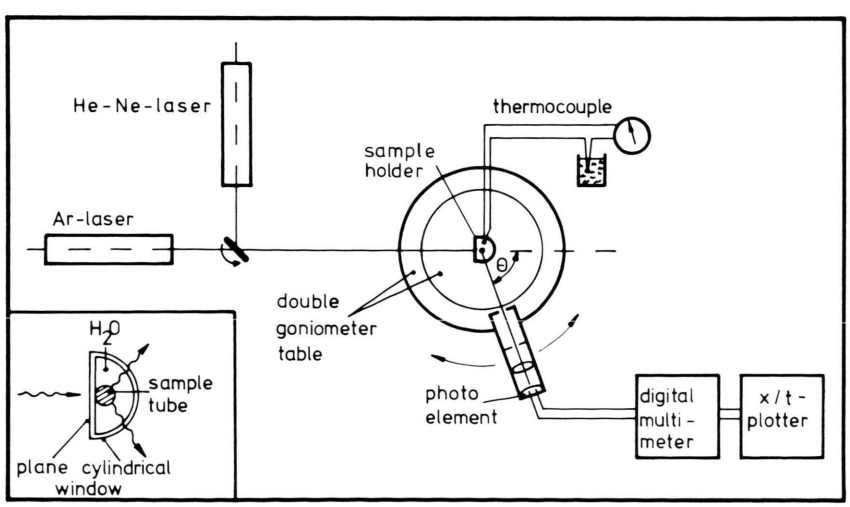

Fig. 1. Arrangement for light diffraction experiments. Inset: Cuvette for sample tubes.

tered beam occuring at the cuvette wall was compensated in first order by the evaluation method, described below.

The second type of cells (type B) had plane-parallel glass windows separated by a distance of ~ 0.8 mm. No immersion cuvette was necessary in this case. While type A cells were always fixed, with the outer, plane window normal to the incident beam, type B cells were either used in a fixed position at an arbitrary angle α to the incident beam or were rotated during the experiment as in the usual single crystal diffraction method. The cells were mounted on a motor-driven Siemens goniometer table (angular resolution ~ 0.05°), which allowed rotation of the photoreceiver (Si photoelements) and, if desired, simultaneously of the cuvette, the latter with half the angular velocity of the receiver.

The diffracted intensity signal was amplified by a Keithley 171 multimeter, the analogue output of which was plotted by an x/t recorder. The synchronization between rotating table and recorder was calibrated for each run. To exclude light that was multi-reflected in the cuvette system, the receiver system was tilted about 20° out of the horizontal plane. An angular resolution of about 0.3° was obtained by using two vertical slits of ~ 1 mm width in front of the receiver.

Evaluation methods

The iridescent gel, consisting of regular layers with periodicity d, gives rise to Bragg reflections which lie on a cone, with aperture angle θ around the direction of the incident beam. θ is given by the Bragg condition

$$\sin \theta/2 = \lambda/(2 \cdot n \cdot d) \tag{1}$$

with λ the wavelength and (in good approximation) n the refractive index of the solution. While θ may be determined directly by experiment if cells of type A are used, multiple refractions of the incident and of the diffracted beam by the cells of type B cause the measured angle δ to differ from θ by

$$\delta = \arcsin (n \cdot \sin [\theta - \arcsin (1/n \sin \alpha)]) + \alpha \tag{2}$$

where α is the angle between cell-window orientation and the direction of the incident beam.

If $\sin(\theta/2)$ is plotted against λ, a straight line is obtained from Eqn (1), the slope of which is mainly determined by d. So, functions $\sin(\theta/2) = A + B \cdot \lambda$ may be found by linear regression and then d may be computed from B. According to Eqn (1), the constant A is expected to be zero and therefore, the actual value of A could be used to check the correct adjustment of the sample. After adjustment the remaining deviations of A from zero were always negligible.

The angular width of the Bragg reflections of our samples was found to be broadened to some degree. The determination of θ from the experimental intensity spectra was difficult in cases where the halfwidth Γ was large. Assuming that this broadening is essentially due to the limited size of coherently scattering regions (Debye-Scherrer-effect), a mean size D of coherently scattering regions (*i.e.* "crystallites") may be determined by

$$D = \lambda/(n \cdot \Gamma \cdot \cos(\theta/2)). \tag{3}$$

The mean number N of layers of TMV rods in a representative crystallite is then obtained by

$$N \simeq D/d. \tag{4}$$

Results

Virus purification

The B & S method always worked well in removing brown substances. Chlorophyll-containing impurities were more difficult to remove, especially with the host plants *Phaseolus vulgaris* and *Cucumis vulgaris* (Table I). Preparations of the other viruses were mostly colorless after 4 differential centrifugations. Pellets after the second or third centrifugation cycle usually showed iridescent diffraction colors. The iridescence was strongest after the third high speed run though the virus was not yet highly purified. Further centrifugations improved the purity but decreased the iridescence and since the purity is not as important for crystallization as monodispersity [16] the latter condition was given preference. Besides, the bottom layer excluded the impurities after some time into an isotropic top layer leaving the ability of the anisotropic layer to crystallize unimpaired.

Of the many other purification methods which we tried, the B & S method was the only reliable one. No iridescence was observed when this method was modified by using 0.1 M Tris-EDTA buffer pH 7.2 [17].

The strongest iridescence was obtained when virus was purified from fresh leaves frozen overnight. Material kept frozen for longer times (1–5 years) gave poor results. All these observations suggest that a high degree of monodispersity is essential for obtaining iridescent gels [11, 18] but is difficult to achieve [19].

In the B & S method, the divalent ions Ca^{2+} and Mg^{2+} which strongly favour end-to-end aggregation were largely removed by EDTA [20] and replaced by Na^{+} [21, 22] during the first purification steps. Conductivity measurements revealed that the ion content decreased during the course of purification from > 2 mS cm^{-1} to about 0.1 mS cm^{-1} in the final virus preparations (20 mg/ml) which corresponds to < 1 mM NaCl. The pH was between 6 and 6.5.

Preparation of iridiscent gels

Stronger iridescence was obtained when the methods of preparing orientated nematic gels for X-ray diffraction were followed [2, 17]. Distilled water was added dropwise to the pellets until a thixotropic gel resulted which could be drawn up in hand-made capillary pipettes or Pasteur pipettes. During the flow into the pipette the initial iridescence became much stronger, indicating a more uniform orientation of the virions (Fig. 2a). When viewed at different angles with respect to the transmitted light, the capillary part of the pipette showed different brilliant uniform Bragg reflection colours from blue to red. The reflection could be seen best when the tube was held vertical and was observed obliquely from above. Observation in polarized light showed that the direction of maximum refractive index was along the long axis.

An increase in ordering could also be obtained by low speed centrifugation. When tubes (2 to 7 mm internal diameter) containing gels were centrifuged in an angle rotor for 15–30 min at 2000 rpm, the strongest reflection was observed along the direction of flow leading to the bottom of the tubes (Fig. 2b). Iridescent gels prepared as described above contained 30–109 mg/ml virus.

Formation and properties of macrocrystals

Macrocrystals up to 2 mm in diameter formed when microcrystalline gels were kept at 0–10 °C in parafilm-sealed tubes of 2 to 7 mm internal diameter (Fig. 2d, e, f). The period over which macrocrystals formed, varied from days to several weeks. Their formation is not fully understood, for of several tubes filled with the same iridescent gel, some developed macrocrystals but others did not. Most experiments were made with TMV, but macrocrystals of all other members of the tobamovirus group (Table II) were obtained and were stable for many months, some for more than 18 months. Crystallization mostly started at the air-liquid interface or at the glass wall. Gels which lost their iridescence could repeatedly form new crystals.

Table II. Mean periodicity d of crystals of six tobacco mosaic viruses.

Virus	Periodicity length d [nm]	Number of measurements
TMV	330 ± 20	12
PTMV	340 ± 20	13
ToMV	340 ± 20	24
CPV	340 ± 20	8
HRV	350 ± 20	4
CV4	370 ± 30	4
ToMV[a]	330 ± 20	6

[a] Virus preparation containing < 1 mM CsCl.

Crystals have a higher density than their environment. This can be concluded from gels of lower concentrations (30 mg/ml) in which the crystals settled to the bottom of the tubes. At higher concentrations, crystals which formed in the upper part of tubes did not settle because of the high viscosity of the gel. They could be sedimented by centrifugation (2000 rpm, 5–30 min).

Whereas iridescent gels were prepared at concentrations of about 100 mg/ml, macrocrystals formed best after dilution with distilled water to concentrations ranging from 70 to 30 mg/ml. Probably, at the higher concentrations, viscosity of the gels hinders macrocrystal formation.

The formation of microcrystalline gels and macrocrystals does not depend primarily on temperature [3, 11, 23]. However, when iridescent gels were heated to 60 °C, an increase in intensity of the reflected light was observed, indicating an increase in crystalline order caused by annealing. When gels were heated to 65–70 °C for 5 min, a white precipitate formed which was birefringent indicating the formation of another paracrystalline phase. After some days at 10 °C the precipitate dissolved and formed new crystals. When heated to > 70 °C for

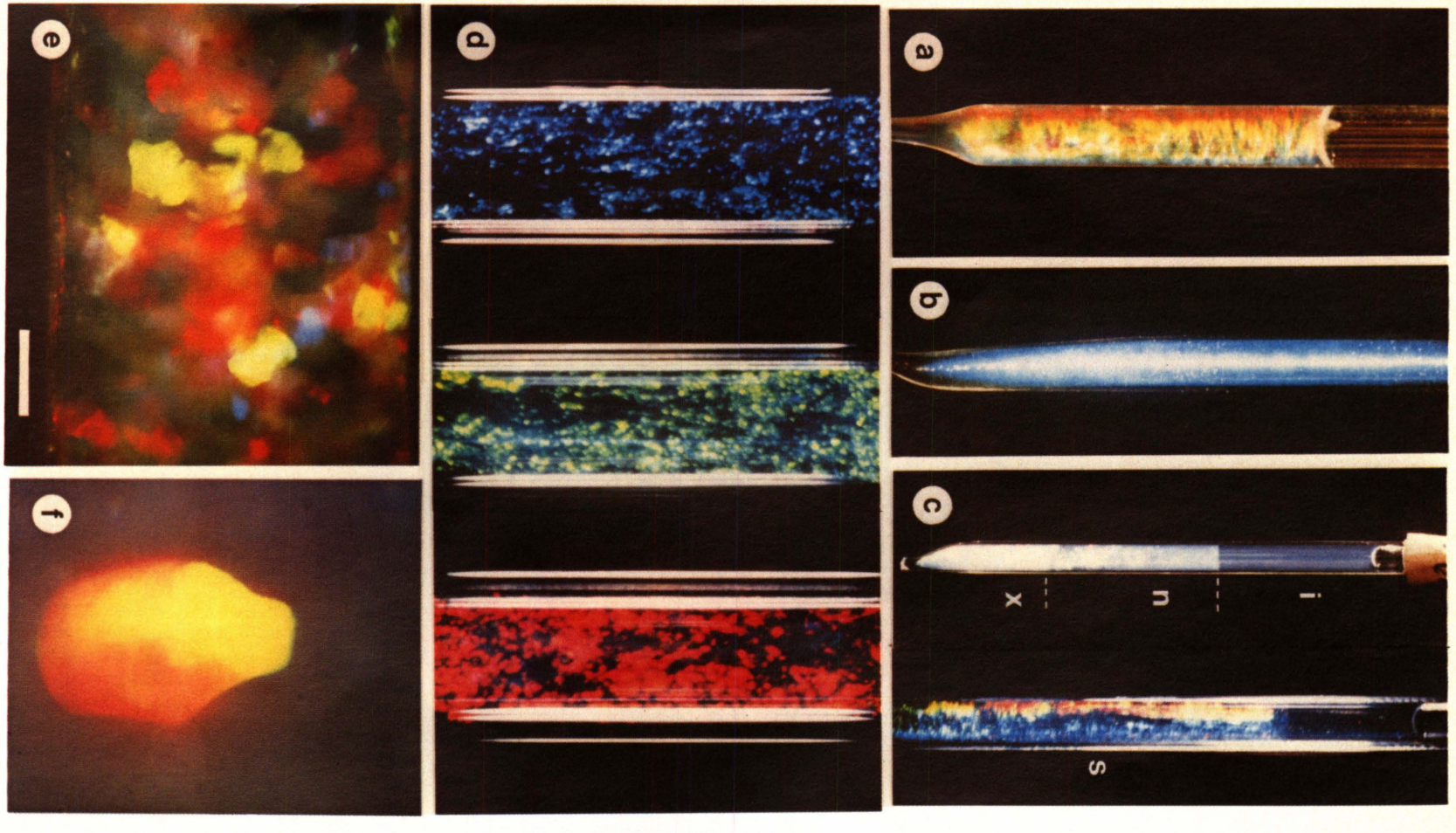

Fig. 2. TMV gels showing diffraction of visible light: a) iridescent gel drawn up in a pipette of 4 mm diameter; b) iridescent gel in a 2 mm tube orientated by centrifugation (2000 rpm, 15 min); c) left: tube with iridescent gel after heating for 5 min at 65 °C followed by centrifugation (2000 rpm, 10 min); i, isotopic phase; n, nematic phase; x, temperature dependent phase); right: the same tube after 2 month at 10 °C, phases n and x have formed the smectic phase s; d) 7 mm tube with macrocrystals (gel at 40 mg/ml) showing different diffraction colors when viewed at different angles of reflection. To avoid multiple reflection, the tubes were placed in water in a plane parallel cuvette; e) macrocrystals in a 2 mm tube showing random crystal orientation. Bar represents 0.5 mm; f) single macrocrystal at higher magnification.

5 min the precipitate became irreversibly insoluble. These effects await further investigation.

In contrast to their thermostability, micro- and macrocrystals were very sensitive to changes in ion concentration. Addition of NaCl (0.001 M) irreversibly destroyed the crystals. Similarly, the bottom layer was destroyed by increased salt concentration [2, 11].

Our samples showed clearly the phase transitions between four mesomorphic phases of TMV which can exist at the same time in a sample tube. The abrupt separation of the nematic (n) from the isotropic (i) phase occurred when the ratio of concentrations c was $c_n/c_i \sim 1.4$, in agreement with the theory of Onsager [3] and the experimental results of Oster [11]. The crystalline gel exhibits a third, smectic, phase (s) which can be sedimented from the nematic phase. Determinations of the concentration made by measuring the refractive index proved that s has a higher concentration than n. For these three phases we observed in a CV4 system the following ratios: $c_n/c_i = 1.4$; $c_s/c_n = 1.15$. The latter estimate may be too low since the single crystals are surrounded by nematic phase. The fourth phase (x), nematic again, was obtained by heating. It had the highest density of all phases and could recrystallize to phase s (Fig. 2c). Thus, the density relationship of the phases was: $c_i < c_n < c_s < c_x$ and for the phase transitions:

$$i \rightarrow n \rightleftharpoons s \overset{t}{\rightleftharpoons} x$$

(t indicates temperature dependent transition).

Light diffraction of various viruses

Usually, large numbers of crystals in random orientation were present in the irradiated volume of the glass tube cells, so the situation resembled that in powder diffraction experiments. In some cases, however, only a few larger macrocrystals contributed to the diffraction.

The plane window cells favoured orientation of the TMV layers of the crystals orthogonal to the windows. Similar orientation was observed in capillary tubes of diameters below 1 mm, where consequently Bragg reflections occurred exclusively in the plane determined by the long tube axis and the direction of incident light. In tubes of greater diameter, the effect was no longer obtained.

Figs. 3a and b show, as an example, two series of angular spectra of the scattered intensity, which

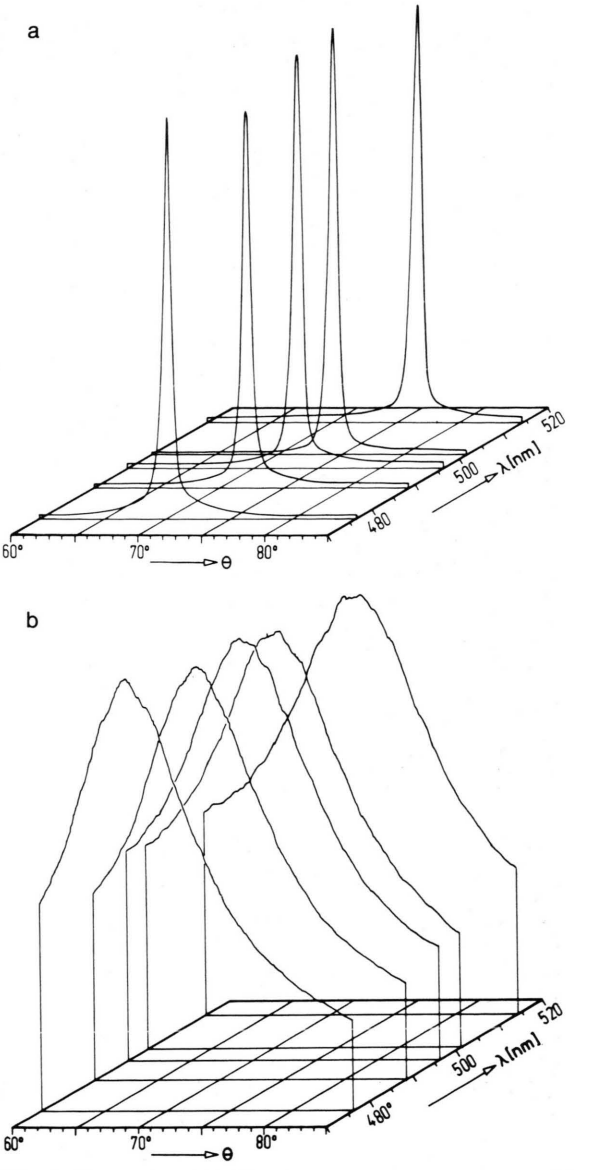

Fig. 3. Examples of diffraction spectra as recorded with 5 Ar-laser wavelengths. Ordinate: light intensity (arbitrary units). a) PTMV macrocrystal sample with extremely small angular width; b) TMV iridescent gel sample with extremely large width. λ: wavelength; θ: angle between incident light and observation direction.

were taken from two samples in type A cells, showing an extremely different halfwidth Γ of the diffraction peak. It should be mentioned that, far away from the peak, the intensity falls below 1% of the maximum in Fig. 3a, *i.e.* there is no distinct scattering background left. Higher order diffraction

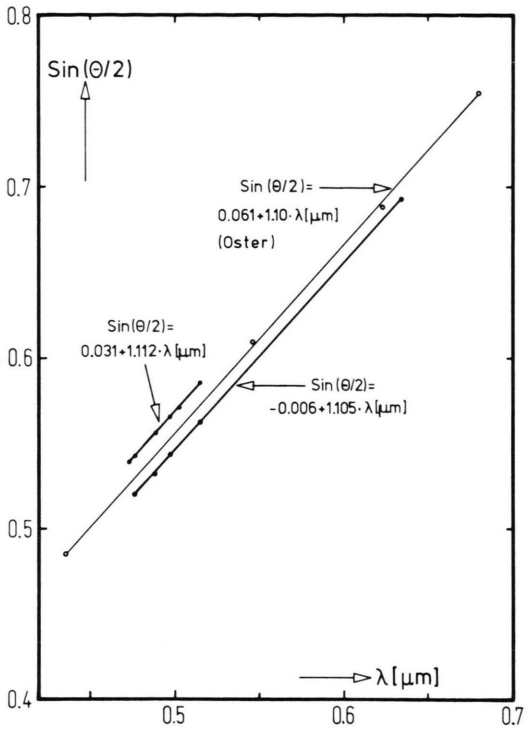

Fig. 4. Plots of the linear function $\sin(\theta/2) = A + B \cdot \lambda$. Full circles: own experiments; open circles: extracted from experimental results of Oster [11].

peaks are absent because the first order θ is already about 70°.

The periodicity d was determined by linear regression. Fig. 4 shows the linear dependence

$$\sin(\theta/2) = f(\lambda)$$

for two samples, and, for comparison, the results given by Oster [11].

The average periodicities of crystals from the various virus strains, as determined from the slopes of these curves, are given in Table II. The value $n = 1.34$ for the refractive index of the solutions was used in the evaluation. All samples compiled in Table II were prepared with concentrations varying from about 30 to 50 mg/ml, and so possible concentration influences on d – as discussed in the following section – were neglected.

As is obvious from Table II, the values of d of all viruses are in full agreement within the given limits of accuracy, the mean value of d being 340 ± 20 nm with the only exception of CV4. However, the latter virus was only partially purified and showed poor iridescence, therefore special systematic errors may have been present in this case.

In conclusion, the periodicities of the crystals of the different viruses had the same value $d = 340 \pm 20$ nm. The length of the virion as determined in the dried state by electron microscopy is 300 nm [14]. Assuming no shrinkage of the virion when dried [2, 24], d may have two components: The length $d' = 300$ nm of the TMV rod plus an additional layer with thickness d'' between the TMV layers in the crystal, presumably consisting of electrolyte solution

$$d = d' + d''. \tag{5}$$

The result is in general agreement with Oster's [11], who found $d = 340$ nm. He used, however, $d' = 280$ nm instead of the above value of Hall [14] which is now generally accepted, and thus obtained $d'' = 60$ nm.

Influences of concentration

To investigate the layer d'' in more detail, additional experiments were performed with TMV and ToMV, varying the concentration of the solution. The samples were prepared by diluting a stock of

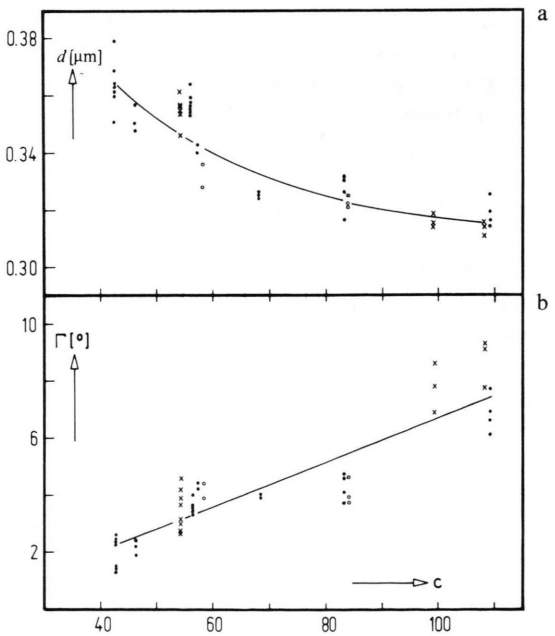

Fig. 5. Experimental results of the concentration dependence of a) the periodicity d and b) the diffraction peak halfwidth Γ. Points: sample series 1; circles: samples series 2; crosses: sample series 3. Vertical groups of signs represent experiments performed at different regions of the same sample tube. c: virus concentration (mg/ml).

iridescent gel with various amounts of water. The concentration of the virus (c) and that of the ions (q) in the solution were thus varied together. Attempts have not yet been made to vary c and q independently.

Iridescent gels were obtained in the concentration range $30 \leq c \leq 109$ mg/ml. Over this range, we found the periodicity d to depend on c as shown in Fig. 5a. This dependence is ascribed to changes of the interlayer distance d'' which, then, increases from 15 nm up to 65 nm. The large scatter is not due to experimental inaccuracies but, rather, to local variations which were observed in different parts of one sample tube as well as in different samples with the same concentration, the sources of which are not clearly understood. The influence of sample temperature can be excluded; it was determined that between 10 °C and 50 °C the periodicity only changed by about 5%.

As a second concentration effect, the halfwidth Γ of the diffraction peak increased markedly with increased c (Fig. 5b). Several explanations will be discussed later.

Discussion

Model calculations for the concentration dependence of d''

The interaction between TMV rods has been discussed repeatedly in the literature. According to Bernal and Fankuchen [2], the paracrystalline phase is the result of electric repulsive and attractive forces. Onsager's theory on phase separation [3] is based solely on electrostatic repulsion between highly anisometric particles. Oster [11] reasoned that repulsive forces lead to a paracrystalline order. To explain the crystal structure of iridescent gels, however, he postulated long-range interaction of both repulsive and attractive nature [18]. The crystal formation of tipula iridescent virus was explained in a similar manner [13].

The last suggestion was supported in our experiments by the observation that crystals in the nematic gel could be sedimented by low speed centrifugation without being destroyed.

We will therefore, in the following, investigate a model of long-range attractive and repulsive forces which yield a bound state in the observed d'' range and a concentration dependence of d''. The following simplifying assumptions are made:

a) The TMV rods form plane layer arrays of thickness d' (rod length) which are stacked regularly with a distance d'' between each layer in the crystal, the rods in neighbouring layers not being tilted against each other as observed *in vivo*.

b) Dipoles are induced in the layers [25] and, notwithstanding the morphological polarity of the rods [26] both sides of each layer are equal in respect to the formation of electric double layers by ions from the electrolyte solution.

c) As was previously discussed the electrolyte solution is assumed to contain only monovalent ions. Possible effects due to polyamines [27, 28] are not considered.

d) The ion concentration of the electrolyte between the rod layers varies on dilution in proportion to the mean concentration outside the crystals.

Then, a combination of Debye-Hückel forces for repulsive and London-van der Waals forces for the attractive interaction may be applied as investigated earlier for inorganic systems of parallel-lying plane layers in an electrolyte solution. The subject is described in detail in the monograph of Verwey and Overbeek [23] and the vast amount of original literature is quoted therein.

For $d'/d'' \gg 1$ the attractive potential is given by

$$V_a = -K_1/d''^2 \tag{6}$$

with

$$K_1 = \text{const} \cdot q_0^2 \cdot \Lambda$$

(q_0 = number of dipoles/cm^3 in the layers; Λ = van der Waals constant).

The repulsive potential due to penetration of Debye-Hückel ion clouds which form double layers near the rod layer surfaces, is, in the approximation of moderate interaction and surface potential, given by

$$V_r = \frac{64\, q_1 \cdot k_B \cdot T}{\varkappa} \exp(-\varkappa \cdot d'') = K_2 \cdot \exp(-\varkappa \cdot d'') \tag{7}$$

with

$$\varkappa = [(8\pi \cdot q_1 \cdot e_0^2)/(\varepsilon \cdot k_B \cdot T)]^{1/2} = \varkappa_0 \cdot q_1^{1/2}$$

(q_1 = number of ions/cm^3 in the solution, far away from the surfaces; k_B = Boltzmann constant; T = abs. temperature; e_0 = elementary charge; ε = dielectric constant of the electrolyte).

Thus, we have for the total interaction potential

$$V = V_a + V_r. \tag{8}$$

The problem is now to determine the concentration dependence of K_1, K_2 and $\varkappa$. Since the different samples were prepared by diluting with water, we assume first that q_1 varies in proportion to the mean virus concentration c. Then, because the potentials given in Eqns (6) and (7) contain q_1 together with constant factors which later will be computed by a fit procedure, we replace q_1 by a variable q, proportional to q_1, the numerical value of which we arbitrarily choose to equal the virus concentration c, which was easily determinable experimentally.

If, then, ε is independent of q (*e.g.* [29]), approximately, we have $\varkappa \propto q^{1/2}$ and $K_2 \propto q^{1/2}$ in Eqn (7).

The independence of K_1 on q, as given by Eqn (6), only holds for solid plates *in vacuo* and is mainly determined by the surface potential which is assumed to be independent of q. In our layers, however, the packing density of the rods surrounded by ions from the electrolyte, depends on q as shown earlier for the nematic phase. Bernal and Fankuchen [2] found for the mean rod distance R within the layers $R \propto 1/c^{1/2}$.

Two extreme cases may thus be distinguished:

a) Rods and ions between them contribute likewise to the van der Waals force (*i.e.* $\Lambda_{\mathrm{TMV}} \approx \Lambda_{\mathrm{ions}}$). Then V_a may be assumed to be approximately independent of q.
b) The TMV rods induce the essential part of the van der Waals interaction (*i.e.* $\Lambda_{\mathrm{TMV}} \gg \Lambda_{\mathrm{ions}}$). Then K_1 of Eqn (6) is proportional to q^2.

Since we did not find distinct arguments to favour one of these dependencies, we will apply both, in the following, using the generalized form for V:

$$V = -k_1 \cdot q^{\nu}/d''^2 + (k_2/\varkappa_0) \cdot q^{1/2} \cdot \exp(-\varkappa_0 \cdot q^{1/2} \cdot d'') \tag{9}$$

where k_1, k_2 and $\varkappa_0$ are constant with respect to q and $\nu = 0$ or $\nu = 2$, respectively.

Being merely interested in the dependence of d'' on q, we may normalize V of Eqn (9) to

$$v = V/k_2 \tag{10}$$

in order to reduce the number of unknown constants. The remaining ones, k_1/k_2 and $\varkappa_0$, then have to be determined by fitting to our experimental results.

This fit procedure was not performed by inserting two selected pairs (d'', q) into Eqn (9) because of the marked sensitivity of V on small variations of d'' within the limits of experimental accuracy. Instead, the experimental values of q at both limits of the stability range, $q_{\min}$ and $q_{\max}$ were used together with d'' at $q = q_{\max}$.

In addition, the following plausible assumptions concerning the shape of the potential curves were made:

a) $dv/dd'' = 0$ for the experimentally determined d'' at $q = q_{\max}$ ("minimum condition") (11)

b) $v^{\mathrm{Min}}(q_{\min}) = v^{\mathrm{Min}}(q_{\max}) - v^{\mathrm{Max}}(q_{\max})$ ("depth condition"). (12)

The superscripts "Min" and "Max" indicate minima and maxima of the $v(d'')$-curves, respectively. The latter condition means that the depths of the potential minima shall coincide at both ends of the stability region (*i.e.* at $q_{\min}$ and $q_{\max}$, respectively). This assumption is plausible, *e.g.*, if these limits are determined by thermal stability; the depth of the potential minima are then of the order of thermal energies.

It should be mentioned, however, that in our samples the observed numerical values of $q_{\max}$ may not only be due to a vanishing long-range binding state but also to influences of the viscosity of the solution which strongly increases with increasing c.

The constants $\varkappa_0$ and k_1/k_2 in the potential of Eqn (10) were obtained by the following iteration method: Since Eqn (11) is explicitely given by

$$k_1/k_2 = d''^3(q_{\max})/q_{\max} \cdot \cdot \exp(-\varkappa_0 \cdot q_{\max}^{1/2} \cdot d''(q_{\max})), \tag{13}$$

k_1/k_2 is determined when some value of $\varkappa_0$ is inserted. With these constants,

$$v^{\mathrm{Min}}(q_{\min}) \quad \text{and} \quad v^{\mathrm{Min}}(q_{\max}) - v^{\mathrm{Max}}(q_{\max})$$

were computed from Eqn (10) and compared to each other. This procedure was reiterated with progressively varied $\varkappa_0$ until the condition Eqn (12) was fulfilled.

Potential curves $v(d'')$ computed from Eqn (10) with these final constants are plotted in Figs. 6 a and b for several values of concentration q. The curves show that for all values of q there is strong attraction if the layer distances are smaller than 5 nm. At large distances, $d'' \gtrsim 100$ nm, all curves asymptotically approach zero. In between, a small potential minimum, marking the stable layer distance d'', exists close to a potential barrier, for $q_{\max} \geq q \geq q_{\min}$.

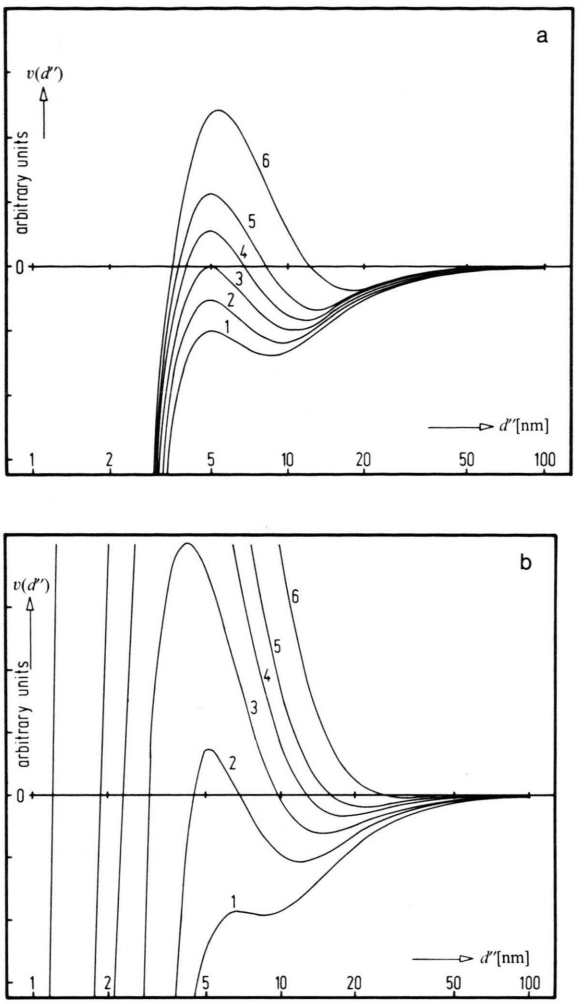

Fig. 6. Interaction potential $v(d'')$ between plane TMV rod layers, plotted against layer distance d''. Parameter: ion concentrations between $q = q_{min}$ (curve 1) and $q = q_{max}$ (curve 6). a): case $v = 0$; b): case $v = 2$.

Mainly due to the concentration dependence of the Debye-Hückel ion cloud (the potential of which is lowered near the layer surface, but extends to larger distances if q is decreased), the position of the minimum strongly varies with q. It is essentially this effect that causes the experimentally observed dependence of the interlayer distance d'' on q.

Values of q larger than q_{max} cause an attractive force for all d'', and, hence, direct aggregation of the TMV rods may occur, while for $q < q_{min}$ the repulsion predominates except for extremely small values of d'', and, hence, no stability is obtained for long-range crystalline structures, both, if $q > q_{max}$ and $q < q_{min}$.

The stability limit at q_{min} is evident from the fact that the potential minimum in our curves becomes too flat beyond q_{min} to prevent the rods from being spread in the paracrystalline phase. The upper q-limit does not appear so obvious; it may be established differently from Eqn (12). Two examples which were investigated numerically, are discussed briefly:

a) The maximum $v^{Max}(q_{max})$ is assumed to be zero. Potential curves including this assumption prove to be highly asymmetric with respect to q, $v^{Min}(q_{max})$ exceeding $v^{Min}(q_{min})$ by more than one order of magnitude, and hence the above assumption appears rather unrealistic for our system.

b) The potential barrier v^{Max} vanishes at $q = q_{max}$, *i.e.* the potential curve has, in this case, an inflection instead of two *extrema.* This case appears most plausible for compact and stiff layers where thermal effects are of minor importance.

A quantitative analysis of these assumptions proved that the q-dependence of the potential mini-

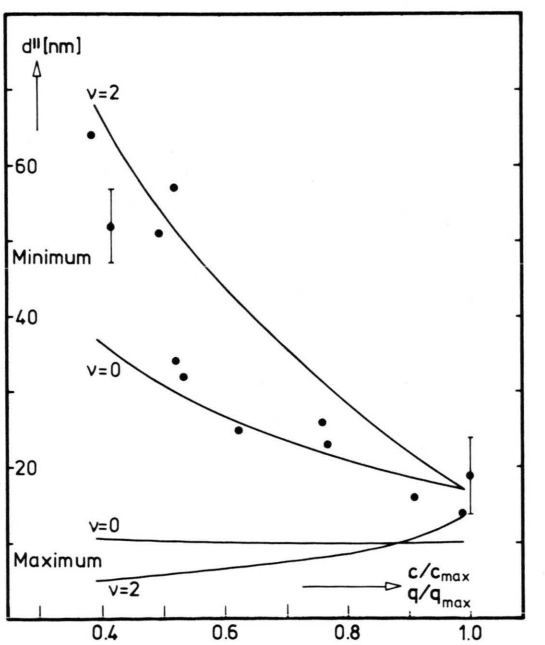

Fig. 7. Positions d'' of the minima and maxima of the computed potential curves in Fig. 6, plotted against concentration q. Points: experimental values of the interlayer distance d'' as determined from diffraction peak positions (each point is the average of all experiments on the same sample).

mum position, *i.e.* the stable interlayer distance (which is the only quantity to be compared with our experimental results), is rather weakly influenced by the special choice of assumptions a), b) or Eqn (12). So, for the following we restrict ourselves to the depth condition of Eqn (12).

A comparison of the potential minimum positions, calculated in this way, with our experimental results for d'' is shown in Fig. 7 for the q region of stable crystalline structures. Obviously, the trend of the experiments is reproduced, giving within the observed stability limits a monotonous decrease of d'' with increasing q. The amount of experimental scatter, however, makes impossible a decision between the cases $v=0$ and $v=2$ (or, possibly, other values of v), and further details concerning the attractive interaction cannot be extracted from the present experiments.

The concentration dependence of Γ

As shown in Fig. 5 b the observed diffraction peak width Γ proved to depend strongly on concentration.

The magnitude of the measured Γ (which is to be considered as an average over many crystallites), may be caused

a) by limited crystal sizes, and/or
b) undulatory local variations of d'' in larger crystals, and/or
c) by size limitations of the coherently scattering regions due to lattice defects, as, *e.g.* multidomain structures.

Assuming the case a) to give the main contribution to Γ, appropriate crystallite sizes may be calculated from Eqns (3) and (4). The approximate mean number of layers N in the crystallites as obtained from the averaged values of Fig. 5 b are plotted in Fig. 8. The corresponding absolute sizes vary from 3 µm to 12 µm. Oster [11] calculated the average thickness of his crystallites to be 5 µm.

The three peak structure in the spectra of Fig. 9 demonstrates that there may exist crystals with slightly different periodicity. Hence, larger Γ may be produced by superimposition of several such crystallites.

Models for the observed concentration dependence of Γ have to be founded on a q dependence of a)–c). Such dependence may be induced via the viscosity of the solution, which strongly increases with c in the region of crystal stability. Probably, the

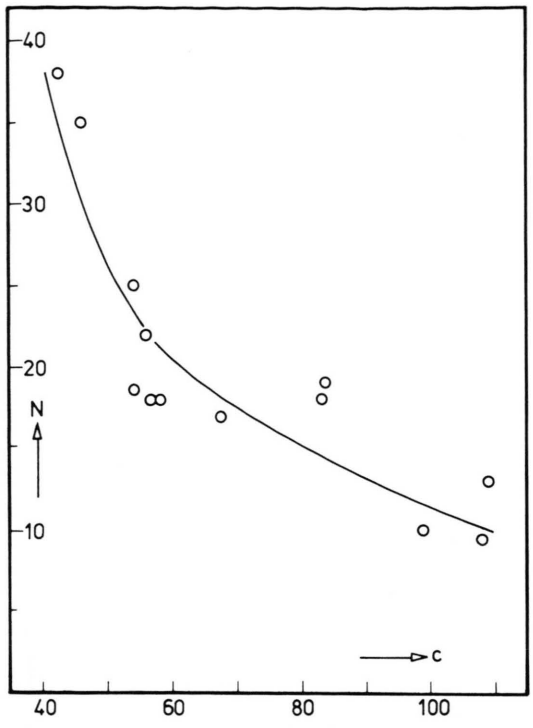

Fig. 8. Mean numbers N of TMV rod layers in the crystallites calculated according to Eqns (3) and (4) from the averaged experimental Γ values of Fig. 5 b, plotted against virus concentration c (mg/ml).

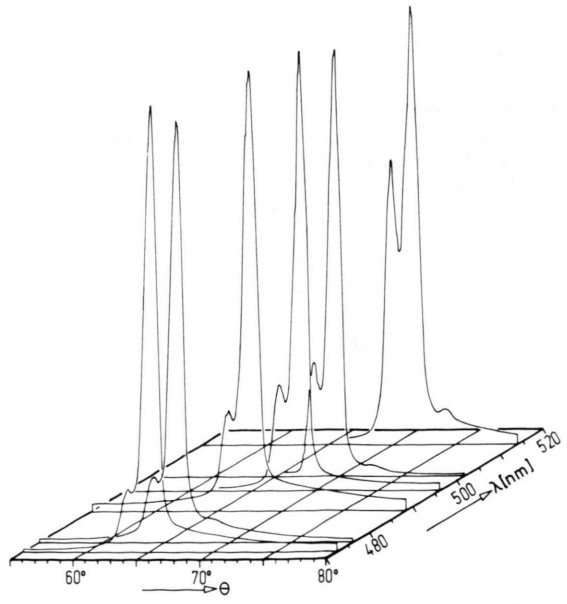

Fig. 9. Diffraction spectra of a TMV sample showing peaks of different crystallites with slightly different periodicity d.

viscosity hinders the exact orientation of the individual TMV rods (case c)) or of the rod layers (case b)). Case b) also may occur due to local inhomogeneities of ion concentration and pH-value within the interlayers and by local deviations from the parallel orientation of rods in adjacent layers.

Case c) may be important since the TMV rods are monodisperse only to a limited extent. According to Hall [14] only 75% of TMV rods prepared by the B & S method have lengths between 290 and 310 nm. Both longer and shorter rods may locally disturb the plane parallel arrangement of the layers.

The potential curves of Fig. 6 also offer a qualitative explanation for the case c). With increasing q, the layers are less tightly bound and this will also hold for the interaction between the neighbouring rods within each layer, since, as mentioned before, their mean distance (and the amount of electrolyte between) also changes with q, as found for the paracrystalline phase [2].

Let us now assume a value of q within the stability region. If, by some means (*e. g.* thermal motion), the distance between two layer regions is diminished below, say, 6 nm, then the attractive potential causes the layers to spontaneously approach till direct contact, and short range forces come into play. Similar effects may occur when single rods or groups of them are moved out of a layer plane. This special kind of lattice defect locally destroys the lattice periodicity, thus causing, via the Debye-Scherrer effect, the half width Γ to increase. Both the weakening of the binding forces within a layer and the reduction of the barrier height of the layer interaction potential with increasing concentration cause a q dependence of the halfwidth, in qualitative agreement with the experimental results.

It is hoped that future investigations will yield further information as to the relative importance of the various theoretical models.

Comparison with in vivo crystals

Crystal types resembling the *in vivo* crystals in optical properties may occur in the living cell, although only rarely [6]. They seem to be uniaxial, with layer distances of 400–320 nm. In contrast, the most common (mature) *in vivo* crystals are hexagonal biaxial plates, with a lateral interparticle distance of about 6 nm [30], a value which may apply also to the layer distance.

Our *in vitro* crystals and the rare type of *in vivo* crystals are apparently similar to early forms of crystals in immature cells as demonstrated in the work of Warmke and Edwardson ([31] *cf.* Figs. 1–5). The fact that TMV can crystallize *in vivo* in a remarkable large number of forms [4–6, 32, 33] suggests that the host cell and the environmental conditions [34] influence the process.

Acknowledgements

We are indebted to Mrs. M. Bernard, Mrs. K. Bompais, and Mr. H. Pressmann for experimental assistance, to Prof. D. G. Schwitzgebel for performing conductivity measurements, to Drs. R. G. Milne and D. Vigren for correcting the manuscript and to those who kindly supplied the virus strains.

[1] F. C. Bawden and N. W. Pirie, Proc. Roy Soc. (London) **123 b,** 274–320 (1937).
[2] J. D. Bernal and I. Fankuchen, J. Gen. Physiol. **25,** 111–165 (1941).
[3] L. Onsager, Ann. New York Acad. Sci. **51,** 627–659 (1949).
[4] H. P. Beale, Contribut. Boyce Thompson Inst. **8,** 413–431 (1937).
[5] F. C. Bawden and F. F. Sheffield, Ann. Appl. Biol. **26,** 102–115 (1939).
[6] M. H. F. Wilkins, A. R. Stokes, W. E. Seeds, and G. Oster, Nature **166,** 127–129 (1950).
[7] R. L. Steere, J. Biophys. Biochem. Cytol. **3,** 45–59 (1957).
[8] W. Wehrmeyer, Naturwissenschaften **44,** 1–3 (1957).
[9] G. J. Hills, Virology **7,** 239–240 (1959).
[10] R. G. Milne, J. Gen. Virol. **1,** 403–404 (1967).
[11] G. Oster, J. Gen. Physiol. **33,** 445–473 (1950).
[12] A. J. Gibbs, CMI/AAB Descriptions of Plant Viruses No. **184,** (1977).
[13] A. Klug, R. E. Franklin, and S. P. F. Humphreys-Owen, Biochim. Biophys. Acta **32,** 203–219 (1959).
[14] C. E. Hall, J. Amer. Chem. Soc. **80,** 2556–2557 (1958).
[15] H. Boedtker and N. S. Simmons, J. Amer. Chem. Soc. **80,** 2550–2556 (1958).
[16] A. Klug and D. L. D. Caspar, Adv. Virus Res. **7,** 225–325 (1960).
[17] J. Gregory and K. C. Holmes, J. Mol. Biol. **13,** 796–801 (1965).
[18] G. Oster, J. Cell. Comp. Physiol. **49,** Suppl. 1, 129–140 (1957).
[19] M. K. Brakke and N. van Pelt, Virology **39,** 516–533 (1969).
[20] W. E. C. Wacker, M. P. Gordon, and J. W. Huff, Biochemistry **2,** 716–719 (1963).
[21] H. S. Loring, Y. Fujimoto, and A. T. Tu, Virology **16,** 30–40 (1962).
[22] H. R. Hulett and H. S. Loring, Virology **25,** 418–430 (1965).
[23] E. J. W. Verwey and J. T. Overbeek, Theory of the Stability of Lyophobic Colloid, Elsevier, Amsterdam 1948.
[24] R. E. Franklin, Biochim. Biophys. Acta **19,** 203–211 (1956).
[25] C. T. O'Konski and A. J. Haltner, J. Amer. Chem. Soc. **79,** 5634–5649 (1957).
[26] T. A. M. Wilson, R. N. Perham, J. F. Finch, and P. J. G. Butler, FEBS Letters **64,** 285–289 (1976).
[27] B. N. Ames and D. T. Dubin, J. Biol. Chem. **235,** 769–775 (1960).
[28] N. W. Johnson and R. Markham, Virology **17,** 276–281 (1962).
[29] J. B. Hasted, Aqueous Dielectris, Chapman and Hall, London 1973.
[30] J. H. M. Willison, J. Ultrastruct. Res. **54,** 176–182 (1976).
[31] H. E. Warmke and J. R. Edwardson, Virology **30,** 45–57 (1966).
[32] R. G. Christie and J. R. Edwardson, Florida Agric. Exp. Sta. Monographs Ser. **9,** (1977).
[33] K. Esau, Viruses in Plant Hosts, Univ. Wis. Press, Madison 1968.
[34] B. Kassanis and F. M. L. Sheffield, Ann. Appl. Biol. **28,** 360–367 (1941).